Biosensors and Bioelectronics 168 (2020) 112559

Contents lists available at ScienceDirect

Biosensors and Bioelectronics

journal homepage: http://www.elsevier.com/locate/bios

# Lateral flow assay modified with time-delay wax barriers as a sensitivity and signal enhancement strategy

Amadeo Sena-Torralba [a,1], Duy Ba Ngo [b,1], Claudio Parolo [a], Liming Hu [a], Ruslan Álvarez-Diduk [a], José Francisco Bergua [a], Giulio Rosati [a], Werasak Surareungchai [b,d], Arben Merkoçi [a,c,*]

[a] Nanobioelectronics & Biosensors Group, Institut Català de Nanociència I Nanotecnologia (ICN2), CSIC and the Barcelona Institute of Science and Technology (BIST), Campus UAB, 08193, Bellaterra, Barcelona, Spain
[b] School of Bioresources and Technology, King Mongkut's University of Technology Thonburi (KMUTT), Bangkok, 10150, Thailand
[c] Catalan Institution for Research and Advanced Studies (ICREA), Pg. Lluís Company 23, 08010, Barcelona, Spain
[d] Nanoscience and Nanotechnology Graduate Research Program, Faculty of Science, KMUTT, Bangkok, 10140, Thailand

ARTICLE INFO

*Keywords:*
Lateral flow
Sensitivity enhancement
Wax barrier
Point-of-Care
Optical biosensor

ABSTRACT

The ease of use, low cost and quick operation of lateral flow assays (LFA) have made them some of the most common point of care biosensors in a variety of fields. However, their generally low sensitivity has limited their use for more challenging applications, where the detection of low analytic concentrations is required. Here we propose the use of soluble wax barriers to selectively and temporarily accumulate the target and label nanoparticles on top of the test line (TL). This extended internal incubation step promotes the formation of the immune-complex, generating a 51.7-fold sensitivity enhancement, considering the limit of quantification, and up to 96% signal enhancement compared to the conventional LFA for Human IgG (H-IgG) detection.

## 1. Introduction

During the last decade we have been observing an ever-growing need for fast and reliable sensing devices for healthcare, environmental and safety applications (Turner, 2013; Malhotra et al., 2005). Both developed and developing countries are increasingly relying on the use of point of care tests (POCT) to keep up with the saturation of their health-care systems, to monitor the quality of their environmental resources and to prevent possible threats. The POCTs represent not only convenient analytical tools for rural regions (they are cheap, portable and easy to use), but they are also establishing themselves as key monitoring devices in the busy centralized areas (Price, 2001; Land et al., 2019; Chin et al., 2012). For example, a faster diagnosis means faster therapy initiation and higher chances to control the spread of a disease; and it also means a quicker response time for starting a remediation campaign in a contaminated river. In this context LFAs are probably the most used POCT covering the widest variety of applications (Quesada-González and Merkoçi, 2015; Posthuma-Trumpie et al., 2009). They serve as an excellent tool for healthcare (Chen et al., 2016; Brangel et al., 2018), safety (Quesada-González et al., 2018; Mirasoli et al., 2012) and environmental applications (Hassan et al., 2019; Schubert-Ullrich et al., 2009; Raeisossadati et al., 2016).

Being fast and easy to use are key features for the POCTs, but they also come with the drawback that their sensitivity has no match with laboratory-based, slower, multi-steps sensing techniques. For example, in the LFA the binding event between bio-receptors (antibodies, aptamers) and their targets happens in the order of seconds (the time required for the flow to pass the TL) (Gasperino et al., 2018; Miller et al., 2018), while in Enzyme-Linked Immunosorbent Assays (ELISA) (Van Weemen and Schuurs, 1971) incubation for several hours is common. Although for many applications the sensitivity of LFAs is sufficient, finding a way to improve it without affecting their being POC devices would open a plethora of new applications. Here we are describing a method to increase the time of the bio-recognition event, without affecting the ease of use and the overall sensing time of the LFAs.

The concept at the base of LFAs, is the use of capillary movement to

* Corresponding author. Nanobioelectronics & Biosensors Group, Institut Català de Nanociència i Nanotecnologia (ICN2), CSIC and The Barcelona Institute of Science and Technology (BIST), Campus UAB, 08193, Bellaterra, Barcelona, Spain.
*E-mail address:* arben.merkoci@icn2.cat (A. Merkoçi).
[1] Amadeo Sena-Torralba and Duy Ba Ngo contributed equally to this work.

https://doi.org/10.1016/j.bios.2020.112559
Received 30 June 2020; Accepted 24 August 2020
Available online 26 August 2020

guide the sample through different functional membranes (Quesada-González and Merkoçi, 2015; Muhammad Sajid et al., 2015). Taking as example an immune-sandwich (non-competitive) assay, first the sample encounters the sample pad, where pre-stored biochemical reagents stabilizes its pH and ionic strength at their optimal values to maximize the signal to noise ratio (Millipore, 2013). Then it flows to the conjugate pad, where the detection antibodies (generally labelled with coloured nanoparticles) recognize the target in the first bio-recognition event (Quesada-González et al., 2019). Then the solution flows along the detection pad, where the complex target/labelled-antibody binds to the capture antibodies of the TL, during the second bio-recognition event. Finally the sample after passing through the control line (CL), reaches the absorbent pad at the end of the LFA. Surprisingly, most of the reported works devoted to improving the sensitivity of LFA have focused on increasing the time for the first bio-recognition event, which depending on the flow-rate of the pads can already take minutes (Zhang et al., 2019; Tsai et al., 2018). However, these approaches not consider the second bio-recognition event, which by being always in the order of seconds represent the real bottleneck for the sensitivity of the test.

The possibility to slow down or even temporarily stop the flow above the test line would increase the time for both bio-recognition events, boosting the sensitivity of the LFAs. Here we present how we achieved it by placing a soluble wax barrier immediately after the TL. Looking at previous works we find that wax structures were previously employed in LFAs just to control the flow (Giokas et al., 2014; Lai et al., 2019; Phillips et al., 2016; Rivas et al., 2014), but never to temporarily stop it. For instance, Preechakasedkit et al. took advantage of wax barriers in order to control the flow of different solutions in lateral flow assay (Preechakasedkita et al., 2018). Besides, some paper-based microfluidic devices did incorporate real barriers to achieve incubation steps, but they were introduced before the test line and were based on salt (He et al., 2019) or sugar (Lutz et al., 2013), which once dissolved can affect the ionic strength of the working buffer and thus the binding reaction. Instead, here, the wax barrier is printed on the surface of the nitrocellulose membrane and melted in order to assure its penetration through the membrane pores creating a hydrophobic barrier just 1 mm after the TL, which is the place where the second bio-recognition event is taking place. The labelled bioreceptor together with the sample flow along the nitrocellulose membrane towards the test line, giving time for the first binding event to occur. Once arrived to the wax barrier, the solution stops temporarily on top of the test line until the barrier breaks, due to the surfactant present on the strip (Fig. 1). In this sense, the thickness of the wax barrier and the concentration of surfactant can be carefully selected in order to modulate the incubation time and determine the optimal conditions to achieve the sensitivity required for the particular application.

## 2. Experimental section

### 2.1. Materials and reagents

Goat anti-human IgG antibody, human IgG, bovine serum albumin (BSA), tetrachloroauric acid ($HAuCl_4$), trisodium citrate, phosphate buffer saline (PBS) tablets, sodium phosphate basic and dibasic, sodium tetraborate, boric acid sucrose and Tween 20 were purchased from Sigma Aldrich (Madrid, Spain). Chicken anti-goat antibody was purchased from Abcam (Cambridge, UK). Human immunoglobulin depleted serum was purchased from Celprogen (Torrance, CA, USA). Nitrocellulose membranes (CN95 and CN150) were purchased from Sartorius Stediem (Göttingen, Germany) and CNPF200 from mdi (Ambala Cantt, India). Cellulose membrane (CFSP001700) was purchased in Merck Millipore (Billerica, MA, USA), glass fiber (Standard 14) from GE Healthcare (Chicago, IL, USA) and supporting adhesive cards were purchased from Kenosha (Amstelveen, The Netherlands). Decol food colorant red powder was purchased in Torten Deko and wax ink (Xerox 108R00935 black) was purchased in Xerox (Norwalk, CT, USA).

### 2.2. Instruments

Wax printer Xerox ColorQube 8580 (Norwalk, CT, USA), IsoFlow

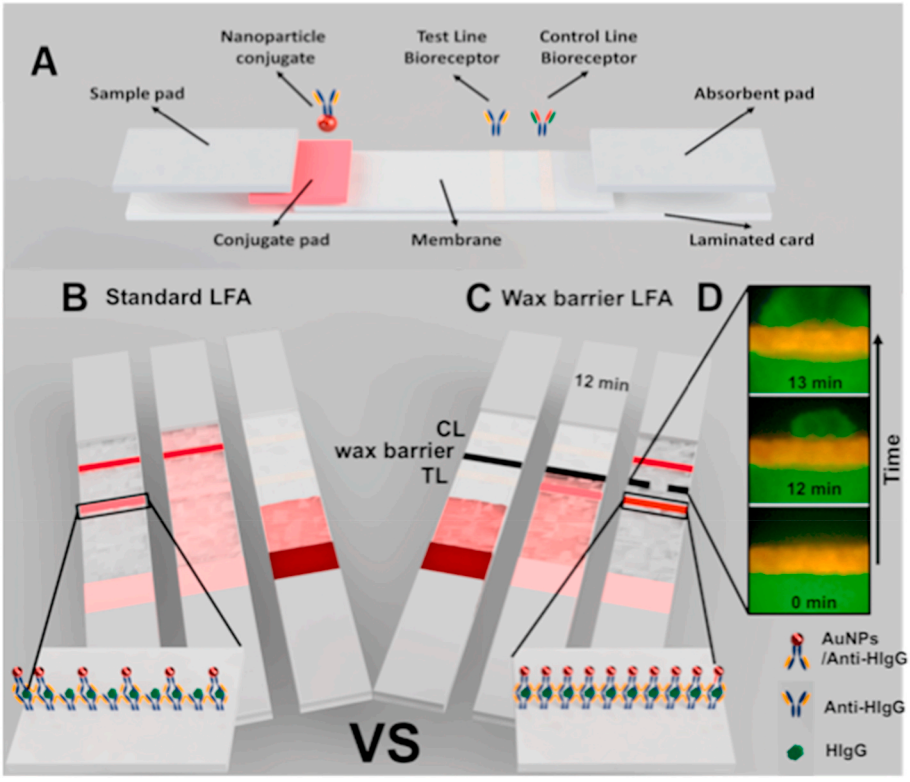


**Fig. 1.** Schematic representation of the proposed strategy for the detection of H-IgG. (A) Scheme of the different pads that make up the LFA strip. (B) In the standard LFA the flow is constantly moving towards the absorbent pad and the bio-recognition event occurs within seconds. Few labelled antibodies are captured in TL, thus the signal intensity is weak. (C) In the LFA modified with a wax barrier, the flow is temporarily stopped on the TL. This increases the time for the bio-recognition event and boosts the assay's sensitivity. (D) Fluorescent microscope pictures (40×) of the wax barrier on the LFA strip. The wax barrier temporarily retains the solution for 12 min. Once broken by the Tween-20, the solution goes through the barrier.

Bioreagent dispenser from Imagene Technology (Hanover, Germany), Microscope Olympus cellSense (Shinjuku, Tokyo, Japan), Centrifuge Allegra 64 R from Beckman Coulter (Brea, CA, USA), Lateral flow strips cutter from Shanghai Kinbio Tech (Pudong New District, Shanghai, China), Spectrophotometer SpectraMax ID3 from Molecular devices (San Jose, CA, USA), SkanMulti from Skannex (Oslo, Norway), TEM Technai F20 (Hillsboro, OR, USA).

### 2.3. Synthesis and characterization of gold nanoparticles

The gold nanoparticles (AuNPs) were synthesized following the Turkevich method (Turkevich et al., 1951). Briefly, 0.5 mL of a $HAuCl_4$ solution (25 mM in MilliQ water) were introduced in a flask containing 49.5 mL of MilliQ water and a magnetic stirrer. The solution was heated to 200 °C under constant and gentle stirring. Once boiling, 1.25 mL of trisodium citrate solution (1% w/v in MilliQ water) were added to the $HAuCl_4$ solution. After 10 min the solution turned to red colour. At this point, the heater was switch off and the solution was left stirring for another 10 min. Once cooled down, the absorbance spectrum of the AuNPs was evaluated with the spectrophotometer. The size and shape of the AuNPs was also characterized by TEM.

### 2.4. Conjugation of the AuNPs with anti H-IgG

The AuNPs were conjugated to antibodies against H-IgG following the procedure previously reported by our group (Ambrosi et al., 2007). Briefly, the pH of the AuNPs solution was adjusted to 8.5 using borate buffer (10 mM pH 8.5). Then, 1.5 mL of the AuNPs solution were mixed with 100 μL of the anti-HIgG solution (100 μg $mL^{-1}$ in PBS buffer 10 mM pH 7.4) and incubated at 650 rpm and 4 °C for 30 min. Next, 100 μL of BSA solution (1% w/v in MilliQ water) were introduced into the conjugate solution and incubated following the same conditions. The excess of antibodies or BSA was removed by centrifugation at 14,000 rpm and 4 °C for 25 min. The pellet was re-suspended in 500 μL of PBS solution (10 mM, pH 7.4, 5% w/v sucrose, 1% w/v BSA and 0.5% v/v tween-20).

### 2.5. Strips fabrication

Firstly, the wax barriers were designed with Inkscape 0.92.3 software, by creating black coloured lines of different thickness (0.01, 0.03, 0.05 and 0.1 mm). Once designed, the document was converted to PDF format and the lines were printed on the nitrocellulose membranes, specifically at 1 mm after the test line. The lines were printed using a wax printer (Xerox ColorQube 8580) and adjusting the resolution to 600 dpi. Then, the nitrocellulose membranes were introduced in the oven, which was pre-heated at 95 °C. 5 min were enough to melt the wax across the nitrocellulose pores, creating an impermeable barrier. The size and morphology of the wax barriers were evaluated by optical microscopy as observed in figure S4.

Secondly, the nitrocellulose membranes were functionalized with anti-HIgG (1 mg $mL^{-1}$ in PBS buffer 10 mM pH 7.4) and chicken to goat antibodies (1 mg $mL^{-1}$ in PBS buffer 10 mM pH 7.4) in test line and control line, respectively. The antibodies deposition was performed with a bioreagent dispenser. Then, the antibodies were fixed on the nitrocellulose membranes by incubating them in the oven at 37 °C for 2 h. In the meantime, the conjugate solution was dispensed on glass fibre and dried in a vacuum chamber at room temperature for 2 h. Moreover, the sample pads were pre-treated by soaking the cellulose membrane in a solution of PBS (10 mM pH 7.4) containing BSA (0.5% w/v) and tween-20 (from 0.05% to 0.1% v/v). They were dried in the oven at 60 °C for 2 h. Finally, the sample, conjugate and absorbent pads were assembled on the laminated cards, which already contained the nitrocellulose membranes. The assembled laminated cards were cut into 0.3 cm-width strips using a dedicated lateral flow cutter.

### 2.6. Assay performance and evaluation

In order to evaluate the retention time achieved with each condition, strips were prepared with different wax barrier widths (0.01, 0.03, 0.05 and 0.1 mm) and Tween-20 concentration in sample pad (0.05, 0.1 and 0.5% v/v). Then, 70 μl of PBS solution (10 mM pH 7.4) was introduced in the wells of a 96 well plate, followed by the immersion of the strips' sample pad. The retention time was measured once the conjugate solution reached the wax barrier. The timer was stopped instantly after the conjugate solution crossed the barrier.

The calibration curves were performed following the same procedure, but using serial dilutions of H-IgG (0, 0.1, 0.3, 1, 3, 10, 30, 100, 300 and 1000 ng $mL^{-1}$) in PBS buffer (10 mM pH 7.4) and in Human immunoglobulin IgG/IgA/IgM/IgE depleted serum. The strips' sample pad was immersed for 20 min and then pictures were taken using a SkanMulti LFA scanner. The pictures were analyzed using Image J software, which enabled the quantification of signal in test line, control line and background.

### 2.7. Stability assay

The stability of the developed lateral flow strips was evaluated by performing an accelerated aging test following the procedure already reported by Wang and co-workers (Wang et al., 2013). The strips were incubated at 37 °C for four weeks and an assay was performed each week for the detection of H-IgG (0, 10, 100, 1000 ng $mL^{-1}$) in human immunoglobulin depleted serum.

## 3. Results and discussion

### 3.1. AuNPs characterization and conjugation to anti H-IgG antibodies

The synthesized AuNPs were firstly characterized by TEM in order to determine its size and distribution. As observed in (figure S1) the AuNPs showed an average diameter of 17.05 nm and a standard deviation of 1.62 nm. We then evaluated the absorbance spectrum of the AuNPs and observed the maximum absorbance peak at 515 nm, as expected (figure S2). Then, we conjugated the AuNPs with antibodies against human IgG following the previously reported procedure (Ambrosi et al., 2007). In order to check if the AuNPs were successfully conjugated with the antibodies, the absorbance spectrum was evaluated. As observed in figure S2, the maximum absorbance peak of the conjugated AuNPs slightly shifted to the right (about 5 nm), indicating the presence of the antibodies on the surface of the AuNPs.

### 3.2. Evaluation of the retention time

When developing the POCT, reproducibility is one of the most important parameters to optimize. For this reason, we fixed the lateral flow strip dimensions to 6 × 0.3 cm and verified that the bed volume corresponds to 70 μL (figure S3). We then proceeded to optimize the barrier fabrication by printing black lines with different widths (0.01, 0.03, 0.05 y 0.1 mm) onto CN95 nitrocellulose membrane, and melting homogeneously the wax at 95 °C for 5 min in the oven (figure S4). Next, we evaluated the time required for breaking the barriers at different concentrations of Tween-20, following the former optimized parameters. In particular, we fabricated lateral flow strips containing different concentrations of Tween-20 (0.05%, 0.1%, 0.5%) in the sample pad and the AuNPs in the conjugate pad. The retention time was measured from the moment at which the AuNPs reached the wax barrier until they crossed the barrier.

As a result, we generated a matrix providing the wax barrier width and Tween-20 concentration that provide different retention times (Table 1 and figure S5). As expected, the retention time rises increasing barrier width and decreasing Tween-20 concentration. In particular, we achieved the longest retention time (12 min) by employing barriers of

**Table 1**
Retention times on CN95 with different wax barrier width and %Tween-20.

| Wax width (mm) | 0.5% Tween-20 | 0.1% Tween-20 | 0.05% Tween-20 |
|---|---|---|---|
| 0.01 | 1.40 ± 0.42 min | 3.93 ± 1.55 min | NB |
| 0.03 | 2.25 ± 0.13 min | 7.64 ± 1.19 min | NB |
| 0.05 | 7.23 ± 0.86 min | 11.45 ± 1.33 min | NB |
| 0.10 | NB | NB | NB |

*NB: No Breaking, which means that the solution dried out before breaking the wax barrier.

0.05 mm and a concentration of Tween-20 of 0.1%; while the shortest retention time (1 min) required a barrier width of 0.01 mm and 0.5% Tween-20. Width of 0.1 mm and Tween-20 concentration of 0.05%, showed to be not suitable for the assay as the barriers broke once the AuNPs solution was already dried out. Moreover, we printed the barriers in a slower flow rate nitrocellulose membrane (CNPF200 mdi), in order to evaluate how the use of smaller pore sizes can affect the retention time. In this case, the pressure applied by the wax printing process compacted the pore of the nitrocellulose, thereby the flow could not even reach the TL.

### 3.3. Evaluation of the sensitivity enhancement in LFA

Finally, after determining the optimum conditions to achieve the longest flow retention, we performed the lateral flow immunoassay for H-IgG detection. In order to check if there is a correlation between the retention time on the TL and the sensitivity enhancement, we fabricated the strips without barriers and with barriers width of 0.01, 0.03 and 0.05 mm. In this regard, we used CN95 and 0.1% Tween-20 as surfactant to break the barriers. We were expecting to see a progressive sensitivity enhancement when using higher width barriers, obtaining the highest sensitivity by using 0.05 mm width barrier, since this is the one that provides the longest retention time. Next, we prepared the strips by fixing anti H-IgG antibodies (1 mg $mL^{-1}$) in the TL and anti-goat antibodies (1 mg $mL^{-1}$) in the CL, both in 10 mM PB buffer pH 7.4. Moreover, we conjugated the AuNPs with anti H-IgG by following the procedure previously reported by our group (Ambrosi et al., 2007), explained in the experimental section. Furthermore, we performed calibration curves using serial dilutions of H-IgG (0 ng $mL^{-1}$ to $10^3$ ng $mL^{-1}$). Finally, we evaluated the signal intensity in both the TL and CL by taking a picture of the strips using a LFA scanner and analyzing them with Image J software (Schneider et al., 2012). We took the pictures of the strips once the AuNPs solution had completely reached the absorbent pad. Eventually, we used the signal values of the TL and the CL after background signal subtraction, and normalized the signal value by dividing TL over CL.

Figure S6 shows the calibration curves obtained when using CN95 and CN150 without the barriers and CN95 with 0.01, 0.03 and 0.05 mm width barriers. As observed the normalized optical intensity increases upon the detection of higher concentrations of H-IgG. Figure S7 shows the pictures of the lateral flow strips after performing the assays. In order to evaluate the sensitivities obtained with each condition we performed a linear fitting from 10 to 1000 ng $mL^{-1}$ and we considered the slope values (Fig. 2A). As expected, a higher sensitivity is achieved when using wider barriers, as this assures a longer interaction time between the antibodies in TL, the labelled antibody and the analyte. The highest sensitivity is achieved when using a 0.05 mm width barrier, which provides a 2.8-fold enhancement compared to the same nitrocellulose without barriers. It is noteworthy that, conversely to the reported, in this specific case, there is not an outstanding sensitivity improvement when reducing the flow rate by using a smaller pore nitrocellulose membrane, as in the case of CN150 (Millipore, 2013; NanoComposix, 2016). Besides, we have proved that the outstanding sensitivity enhancement is obtained only when temporarily stopping the flow above the TL.

Moreover, we calculated the limit of detection (LoD) and quantification (LoQ) achieved for every tested condition. The LoD was calculated as $Optical\ intensity_{LOD} = blank + 3\,\sigma_{blank}$ (i.e. the corresponding value of blank sample plus 3 times its standard deviation) (Armbruster and Pry, 2008). The LoD for CN95, CN150 and CN95 with 0.01, 0.03 and 0.05 mm width barriers were 35.01, 73.23, 21.67, 18.71, 14.47 ng $mL^{-1}$, respectively. Furthermore, the LoQ, calculated as $Optical\ intensity_{LOD} = blank + 10\,\sigma_{blank}$, were 2129.09, 1909.76, 1164.38, 87.49, 41.19 ng $mL^{-1}$, respectively. We obtained the lowest LoD and LoQ values by setting the barriers at the condition that permitted the highest retention time of the conjugate solution on the TL. With that condition we achieved a 2.4-fold and 51.7-fold sensitivity enhancement compared to the unmodified LFA, when comparing the LoDs and LoQs, respectively. These values are quite competitive when compared to the ones reported in other approaches devoted to H-IgG detection (Table S1).

In Fig. 2B, we show pictures of the LFA strips after performing the calibration curve assay from 10 to 1000 ng $mL^{-1}$ using CN95, CN150 non-modified with the wax barriers and CN95 modified with 0.01, 0.03 and 0.05 mm width barriers. As observed, there is a signal enhancement in TL when introducing the wax barriers in to the system. The percentage signal enhancement was calculated taking as reference the

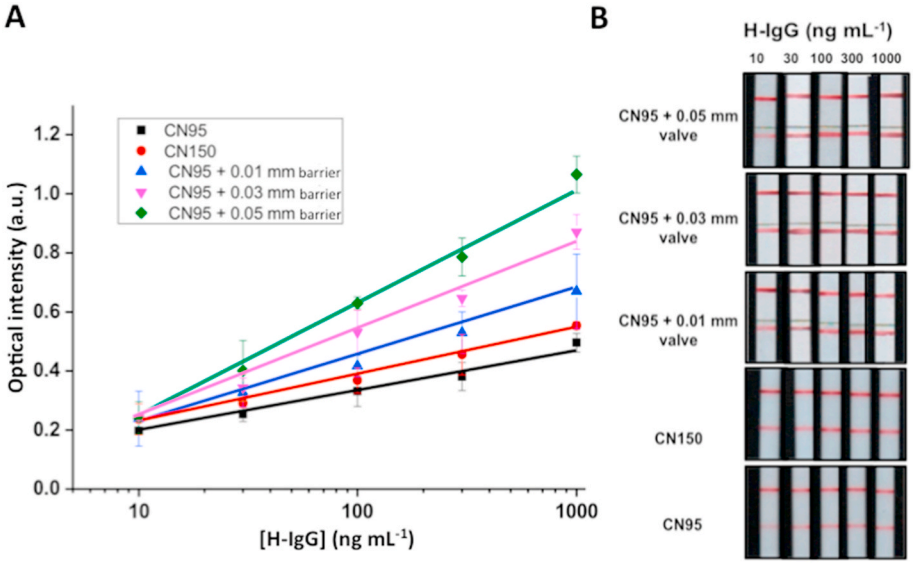


**Fig. 2.** The LFA for H-IgG detection using time-delay barriers. **(A)** Calibration curve from 10 to 1000 ng $mL^{-1}$ showing the optical intensity linear range when using CN95 (Optical intensity = 0.0631 ln [H-IgG (ng $mL^{-1}$)] + 0.0433 $R^2$ = 0.98) and CN150 non-modified with the wax barriers (Optical intensity = 0.0695 ln [H-IgG (ng $mL^{-1}$)] + 0.0627 $R^2$ = 0.99) and CN95 modified with 0.01 (Optical intensity = 0.0925 ln [H-IgG (ng $mL^{-1}$)] + 0.0124 $R^2$ = 0.99), 0.03 (Optical intensity = 0.1359 ln [H-IgG (ng $mL^{-1}$)] - 0.1165 $R^2$ = 0.96) and 0.05 mm width barriers (Optical intensity = 0.1767 ln [H-IgG (ng $mL^{-1}$)] - 0.2056 $R^2$ = 0.98). **(B)** Pictures of the LFA strips after performing the calibration curve assay from 10 to 1000 ng $mL^{-1}$ using CN95, CN150 non-modified with the wax barriers and CN95 modified with 0.01, 0.03 and 0.05 mm width barriers.

normalized optical intensity of the strips with CN95 and without the wax barriers (Table S2). As observed, the percentage signal increase is higher for increasing concentrations of H-IgG. The highest percentage signal increase is 96%, and was achieved for 1000 ng $mL^{-1}$ when using CN95 with a 0.05 mm width barrier.

Finally, we proved that a longer incubation time of the conjugate solution over the TL did not favour the generation of non-specific signal in TL. As shown in figure S8, the signal in TL for blank samples (0 ng $mL^{-1}$ of H-IgG) is not higher when using wider wax barriers, as we obtained the highest TL signal for the blank sample when using the CN150 nitrocellulose membrane. We also proved that the assay performance is better when fixing the wax barrier after the TL than before the TL. We compared the calibration curves for H-IgG detection (0–$10^3$ ng $mL^{-1}$) in PBS buffer obtained using CN95 lateral flow assay strips modified with 0.05 mm width barrier at 1 mm before and after the TL. As observed in figure S9, the normalized optical intensity is higher at low concentrations of H-IgG when fixing the wax barrier after the TL, favouring the direct inspection by naked eye. In addition, the achieved LoD is also lower with the barrier after the TL (14 versus 22 ng $mL^{-1}$) when adjusting a logarithmic fitting from 30 to $10^3$ ng $mL^{-1}$.

### 3.4. Assay with human serum

Once we proved that the proposed sensitivity enhancement strategy was working, the next step was to test the assay's applicability with real samples. We decided to perform the assay in human serum, as it is one of the most common applied samples in diagnosis (Trost, 2014). Besides, our LFA has been developed for the detection of general H-IgG (non-specific for a particular disease), which appears at a concentration ranging from 3 to 16 mg $mL^{-1}$ in the human serum (Cassidy and Nordby, 1975). Given the fact that this concentration is far away from the linear range of the calibration curve (see Fig. 2A), we performed the validation assay by spiking different concentrations of H-IgG (0–$10^3$ ng $mL^{-1}$) in immunoglobulins depleted human serum. The use of IgG depleted human serum does not detract the relevance of the validation assay as firstly, the samples used are still based on a complex matrix (immunoglobulins only stand for the 10–20% of the protein content in human serum) (Leeman et al., 2018) and secondly, the use of this type of serum has already been used in other reports for assay validation (Cheeveewattanagul et al., 2017; Zamora-Gálvez et al., 2018).

We performed the calibration curve in human serum using the conditions that provide the highest retention time (0.05 mm width barrier and 0.1% tween-20) and therefore the highest sensitivity and compared the results with the ones obtained in buffer medium (Fig. 3). The calibration curve in human serum followed the same trend as in buffer medium, with a correlation of 0.98 in the linear range (10–$10^3$ ng $mL^{-1}$). Besides, the normalized optical intensity slightly decreased at low concentrations of H-IgG, which is related to the matrix effect commonly reported in immunoassays (Rosenberg-Hasson et al., 2014). However, this not affected the analytical performance of our platform, since the LoD in human serum remained similar to the one achieved with buffer medium (17.70 and 14.47 ng $mL^{-1}$, respectively). In addition, the blank samples did not cause an increase in the normalized optical intensity, thus no cross-reactivity or non-specific interactions were observed with the matrix components. Finally, recovery test was performed spiking three concentrations of H-IgG within the linear range of the calibration curve, in standard buffer and immunoglobulin-depleted serum. It was found that the recovery percentage ranged from 86 to 122%, indicating that the complex matrix of the human serum did not affect the reliability of the proposed LFA (Table S3).

### 3.5. Repeatability and stability

Finally, we performed repeatability and stability assays so as to demonstrate the applicability of the proposed platform in real scenarios. Regarding the repeatability, we prepared three different batches of LFA strips using CN95 nitrocellulose membrane with 0.05 mm width wax barrier after TL. We performed the detection of four concentrations of H-IgG (0, 10, 100 and 1000 ng $mL^{-1}$) spiked in immunoglobulin depleted human serum and determined the coefficient of variation (CV) of the different batches. These values were obtained by calculating the ratio of the standard deviation to the average signal. As observed in Table S4 the CV values for concentrations of H-IgG lower than the LoD (17.70 ng $mL^{-1}$) were higher than 15%, while the CV values for 100 and 1000 ng $mL^{-1}$ were lower than 10%, which is the recommended value in immunoassays (Grotjan and Keel, 1996).

Moreover, in order to evaluate the long-term performance of our platform we performed an accelerated aging test following the procedure reported by (Wang et al., 2013). Briefly, we stored the CN95 nitrocellulose membrane strips modified with 0.05 mm width wax barrier after TL at 37 °C for 0–4 weeks and detected different concentrations of H-IgG (0, 10, 100 and 1000 ng $mL^{-1}$) spiked in immunoglobulin depleted human serum every week. Fig. 4 A shows the optical intensity values obtained with the strips being stored for 2, 3 and 4 weeks at 37 °C. The CV values were lower than 10% for all the evaluated concentrations (Table S5), meaning that the developed strips are stable for at least 4 months at 25 °C. This can also be observed in Fig. 4 B, where the differences in signal intensity in TL and CL are negligible when inspected by naked eye.

## 4. Conclusion

In conclusion, we have developed a LFA modified with time-delay barriers as a strategy for sensitivity and signal enhancement. We have achieved an inner incubation time of 12 min, which produced a 51.7-fold enhancement in sensitivity, considering the LoQ and up to 96% signal enhancement. The assay proved excellent applicability with immunoglobulin depleted human serum. We believe the proposed

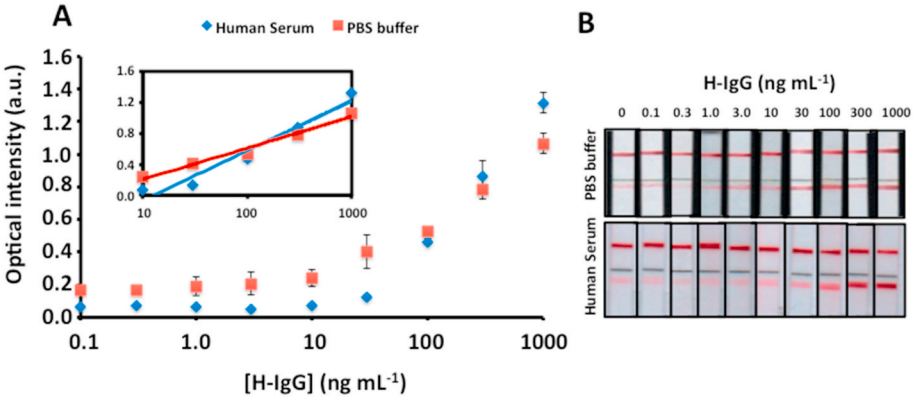


**Fig. 3.** Validation assay with immunoglobulin depleted human serum. **(A)** Calibration curve for H-IgG detection (0–$10^3$ ng $mL^{-1}$) in human serum (blue) and PBS buffer (red) using CN95 nitrocellulose membrane strips modified with 0.05 mm width wax barrier after TL. Inset of the logarithmic fitting from 10 to $10^3$ ng $mL^{-1}$ in human serum (Optical intensity = 0.2804 ln [H-IgG (ng $mL^{-1}$)] - 0.716 $R^2$ = 0.95) and in PBS buffer (Optical intensity = 0.1767 ln [H-IgG (ng mL-1)] + 0.2056 $R^2$ = 0.97). **(B)** Pictures of the strips after performing the calibration curve assay in human serum and PBS buffer. (For interpretation of the references to colour in this figure legend, the reader is referred to the Web version of this article.)

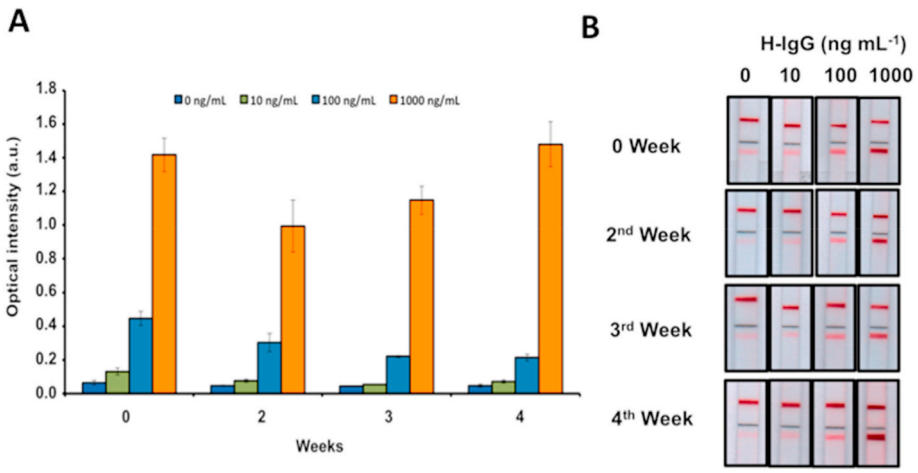


**Fig. 4.** Stability assay. **(A)** Optical intensity values for the detection of 0, 10, 100 and 1000 ng $mL^{-1}$ of H-IgG in immunoglobulin depleted human serum, using LFA strips stored at 37 °C for 0–4 weeks. **(B)** Pictures of the LFA strips after performing the stability assay.

method represents an outstanding solution to improve the analytical performance of LFAs, without sacrificing their ease-of-use and low cost. In addition, the proposed strategy can be really interesting in applications where high sensitivity is required, and also in assays where the bioreceptors used, require more interaction time with the target analyte, such as antibodies with lower affinity or nucleic-acid based probes.

## Credit author statement

**Amadeo Sena-Torralba:** Methodology, Investigation, Validation and Writing - Original Draft **Duy Ba Ngo:** Methodology, Investigation, Validation and Writing - Review & Editing **Claudio Parolo:** Conceptualization, Methodology, Supervision, Writing - Original Draft and Writing - Review & Editing, **Liming Hu:** Validation and Writing - Review & Editing **Ruslan Álvarez-Diduk:** Investigation and Writing - Review & Editing **José Francisco Bergua:** Methodology and Writing - Review & Editing **Giulio Rosati:** Supervision and Writing - Review & Editing **Werasak Surareungchai:** Supervision and Writing - Review & Editing **Arben Merkoçi:** Supervision, Writing - Review & Editing and Funding acquisition.

## Declaration of competing interest

The authors declare that they have no known competing financial interests or personal relationships that could have appeared to influence the work reported in this paper.

## Acknowledgments

We acknowledge financial support from NACANCELL project PCIN-2016-066 (program Euronanomed 2). This work is also funded by the CERCA Program/Generalitat de Catalunya. The ICN2 is funded by the CERCA programme/Generalitat de Catalunya. ICN2 acknowledges the support of the Spanish MINECO for the Project MAT 2017-87202-P and through the Severo Ochoa Centres of Excellence Program under Grant SEV2201320295. Amadeo Sena-Torralba acknowledge Autonomous University of Barcelona (UAB) for the possibility of performing this work inside the framework of Biotechnology Ph.D. Programme. Duy Ba Ngo gratefully acknowledges Petchra Pra Jom Klao Doctoral, King Mongkut's University of Technology Thonburi (KMUTT) in Thailand and Sensor Technology, School of Bioresources and Technology, KMUTT, Thailand.

## Appendix A. Supplementary data

Supplementary data to this article can be found online at https://doi.org/10.1016/j.bios.2020.112559.

## References

Ambrosi, A., Castañeda, M.T., Killard, A.J., Smyth, M.R., Alegret, S., Merkoçi, A., 2007. Double-codified gold nanolabels for enhanced immunoanalysis. Anal. Chem. 79, 5232–5240.

Armbruster, D.A., Pry, T., 2008. Limit of blank, limit of detection and limit of quantitation. Clin. Biochem. Rev. 29 (Suppl. 1), S49–S52.

Brangel, P., Sobarzo, A., Parolo, C., Miller, B.S., Howes, P.D., Gelkop, S., Lutwama, J.J., Dye, J.M., McKendry, R.A., Lobel, L., Stevens, M.M., 2018. A serological point-of-care test for the detection of IgG antibodies against ebola virus in human survivors. ACS Nano 12, 63–73. https://doi.org/10.1021/acsnano.7b07021.

Cassidy, J.T., Nordby, G.L., 1975. Human serum immunoglobulin concentrations: prevalence of immunoglobulin deficiencies. J. Allergy Clin. Immunol. 55, 35–48. https://doi.org/10.1016/S0091-6749(75)80006-6.

Cheeveewattanagul, N., Morales-Narváez, E., Hassan, A.R.H.A., Bergua, J.F., Surareungchai, W., Somasundrum, M., Merkoçi, A., 2017. Straightforward immunosensing platform based on graphene oxide-decorated nanopaper: a highly sensitive and fast biosensing approach. Adv. Funct. Mater. 27, 1–8. https://doi.org/10.1002/adfm.201702741.

Chen, Y., Sun, J., Xianyu, Y., Yin, B., Niu, Y., Wang, S., Cao, F., Zhang, X., Wang, Y., Jiang, X., 2016. A dual-readout chemiluminescent-gold lateral flow test for multiplex and ultrasensitive detection of disease biomarkers in real samples. Nanoscale 8, 15205–15212. https://doi.org/10.1039/c6nr04017a.

Chin, C.D., Linder, V., Sia, S.K., 2012. Commercialization of microfluidic point-of-care diagnostic devices. Lab Chip 12, 2118–2134. https://doi.org/10.1039/c2lc21204h.

Gasperino, D., Baughman, T., Hsieh, H.V., Bell, D., Weigl, B.H., 2018. Improving lateral flow assay performance using computational modeling. Annu. Rev. Anal. Chem. 11, 219–244. https://doi.org/10.1146/annurev-anchem-061417-125737.

Giokas, D.L., Tsogas, G.Z., Vlessidis, A.G., 2014. Programming fluid transport in paper-based microfluidic devices using razor-crafted open channels. Anal. Chem. 86, 6202–6207. https://doi.org/10.1021/ac501273v.

Grotjan, E.H., Keel, B.A., 1996. Data interpretation and quality control. In: Diamandis, E. P., Christopoulos, T.K. (Eds.), Immunoassay. Academic Press, San Diego, pp. 51–94.

Hassan, A.H.A., Bergua, J.F., Morales-Narváez, E., Mekoçi, A., 2019. Validity of a single antibody-based lateral flow immunoassay depending on graphene oxide for highly sensitive determination of E. coli O157:H7 in minced beef and river water. Food Chem. 297, 124965. https://doi.org/10.1016/j.foodchem.2019.124965.

He, X., Liu, Z., Yang, Y., Li, L., Wang, L., Li, A., Qu, Z., Xu, F., 2019. Sensitivity enhancement of nucleic acid lateral flow assays through a physical-chemical coupling method: dissoluble saline barriers. ACS Sens. 4, 1691–1700. https://doi.org/10.1021/acssensors.9b00594.

Lai, Y., Tsai, C., Hsu, J., Lu, Y., 2019. Microfluidic time-delay valve mechanism on paper-based devices for automated competitive ELISA. Micromachines 10, 837.

Land, K.J., Boeras, D.I., Chen, X.S., Ramsay, A.R., Peeling, R.W., 2019. REASSURED diagnostics to inform disease control strategies, strengthen health systems and improve patient outcomes. Nat. Microbiol. 4, 46–54. https://doi.org/10.1038/s41564-018-0295-3.

Leeman, M., Choi, J., Hansson, S., Storm, M.U., Nilsson, L., 2018. Proteins and antibodies in serum, plasma, and whole blood—size characterization using asymmetrical flow field-flow fractionation (AF4). Anal. Bioanal. Chem. 410, 4867–4873. https://doi.org/10.1007/s00216-018-1127-2.

Lutz, B., Liang, T., Fu, E., Ramachandran, S., Kauffman, P.Y.P., 2013. Dissolvable fluidic time delays for programming multi-step assays in instrument-free paper diagnostics. Lab Chip 13, 2840–2847. https://doi.org/10.1038/jid.2014.371.

Miller, B.S., Parolo, C., Turbé, V., Keane, C.E., Gray, E.R., McKendry, R.A., 2018. Quantifying biomolecular binding constants using video paper analytical devices. Chem. Eur J. 24, 9783–9787. https://doi.org/10.1002/chem.201802394.

Millipore, M., 2013. Rapid Lateral Flow Test Strips Considerations for Product Development.

Mirasoli, M., Buragina, A., Dolci, L.S., Guardigli, M., Simoni, P., Montoya, A., Maiolini, E., Girotti, S., Roda, A., 2012. Development of a chemiluminescence-based quantitative lateral flow immunoassay for on-field detection of 2,4,6-trinitrotoluene. Anal. Chim. Acta 721, 167–172. https://doi.org/10.1016/j.aca.2012.01.036.

NanoComposix, 2016. Lateral Flow Assay Development Guide. nanoComposix Lateral Flow Handb v.1.4.

Phillips, E.A., Shen, R., Zhao, S., Linnes, J.C., 2016. Thermally actuated wax valves for paper-fluidic diagnostics. Lab Chip 16, 4230–4236. https://doi.org/10.1039/c6lc00945j.

Posthuma-Trumpie, G.A., Korf, J., Van Amerongen, A., 2009. Lateral flow (immuno) assay: its strengths, weaknesses, opportunities and threats. A literature survey. Anal. Bioanal. Chem. 393, 569–582. https://doi.org/10.1007/s00216-008-2287-2.

Preechakasedkita, P., Siangprohb, W., Khongchareonpornc, N., Ngamrojanavanichc, N., Chailapakul, O., 2018. Development of an automated wax-printed paper-based lateral flow device for alpha-fetoprotein enzyme-linked immunosorbent assay. Biosens. Bioelectron. 102, 27–32.

Price, C.P., 2001. Regular review: point of care testing. Br. Med. J. 322, 1285–1288. https://doi.org/10.1136/bmj.322.7297.1285.

Quesada-González, D., Merkoçi, A., 2015. Nanoparticle-based lateral flow biosensors. Biosens. Bioelectron. 73, 47–63. https://doi.org/10.1016/j.bios.2015.05.050.

Quesada-González, D., Jairo, G.A., Blake, R.C., Blake, D.A., Merkoçi, A., 2018. Uranium (VI) detection in groundwater using a gold nanoparticle/paper-based lateral flow device. Sci. Rep. 8, 8–15. https://doi.org/10.1038/s41598-018-34610-5.

Quesada-González, D., Sena-Torralba, A., Wicaksono, W.P., de la Escosura-Muñiz, A., Ivandini, T.A., Merkoçi, A., 2019. Iridium oxide (IV) nanoparticle-based lateral flow immunoassay. Biosens. Bioelectron. 132, 132–135. https://doi.org/10.1016/j.bios.2019.02.049.

Raeisossadati, M.J., Danesh, N.M., Borna, F., Gholamzad, M., Ramezani, M., Abnous, K., Taghdisi, S.M., 2016. Lateral flow based immunobiosensors for detection of food contaminants. Biosens. Bioelectron. 86, 235–246. https://doi.org/10.1016/j.bios.2016.06.061.

Rivas, L., Medina-Sánchez, M., de la Escosura-Muñiz, A., Merkoçi, A., 2014. Improving sensitivity of gold nanoparticle-based lateral flow assays by using wax-printed pillars as delay barriers of microfluidics. Lab Chip 14, 4406–4414. https://doi.org/10.1039/c4lc00972j.

Rosenberg-Hasson, Y., Hansmann, L., Liedtke, M., Herschmann, I., Maecker, H.T., 2014. Effects of serum and plasma matrices on multiplex immunoassays. Immunol. Res. 58, 224–233. https://doi.org/10.1007/s12026-014-8491-6.

Sajid, Muhammad, Abdel-Nasser, Kawde, Daud, Muhammad, 2015. Designs, formats and applications of lateral flow assay: a literature review. J. Saudi Chem. Soc 19, 689–705. https://doi.org/10.1016/J.JSCS.2014.09.001.

Schneider, C.A., Rasband, W.S., Eliceiri, K.W., 2012. NIH Image to ImageJ: 25 years of image analysis. Nat. Methods 9, 671–675. https://doi.org/10.1038/nmeth.2089.

Schubert-Ullrich, P., Rudolf, J., Ansari, P., Galler, B., Führer, M., Molinelli, A., Baumgartner, S., 2009. Commercialized rapid immunoanalytical tests for determination of allergenic food proteins: an overview. Anal. Bioanal. Chem. 395, 69–81. https://doi.org/10.1007/s00216-009-2715-y.

Trost, D.C., 2014. Hepatotoxicity. In: Lawrence Gould, A. (Ed.), Statistical Methods for Evaluating Safety in Medical Product Development. John Wiley & Sons, Ltd, New Jersey, pp. 229–270.

Tsai, T.T., Huang, T.H., Chen, C.A., Ho, N.Y.J., Chou, Y.J., Chen, C.F., 2018. Development a stacking pad design for enhancing the sensitivity of lateral flow immunoassay. Sci. Rep. 8, 1–10. https://doi.org/10.1038/s41598-018-35694-9.

Turkevich, J., Stevenson, P.C., Hillier, J., 1951. A study of the nucleation and growth processes in the synthesis of colloidal gold. Discuss. Faraday Soc. 11, 55–75.

Turner, A.P.F., 2013. Biosensors: sense and sensibility. Chem. Soc. Rev. 42, 3184–3196. https://doi.org/10.1039/c3cs35528d.

Wang, D.B., Tian, B., Zhang, Z.P., Deng, J.Y., Cui, Z.Q., Yang, R.F., Wang, X.Y., Wei, H.P., Zhang, X.E., 2013. Rapid detection of Bacillus anthracis spores using a super-paramagnetic lateral-flow immunological detection system. Biosens. Bioelectron. 42, 661–667. https://doi.org/10.1016/j.bios.2012.10.088.

Van Weemen, B.K., Schuurs, A.H.W.M., 1971. Immunoassay using antigen-enzyme conjugates. FEBS Lett. 15, 232–236. https://doi.org/10.1016/0014-5793(71)80319-8.

Zamora-Gálvez, A., Morales-Narváez, E., Romero, J., Merkoçi, A., 2018. Photoluminescent lateral flow based on non-radiative energy transfer for protein detection in human serum. Biosens. Bioelectron. 100, 208–213. https://doi.org/10.1016/j.bios.2017.09.013.

Zhang, S.F., Liu, L.N., Tang, R.H., Liu, Z., He, X.C., Qu, Z.G., Li, F., 2019. Sensitivity enhancement of lateral flow assay by embedding cotton threads in paper. Cellulose 26, 8087–8099. https://doi.org/10.1007/s10570-019-02677-6.